Astronomy & Astrophysics

LETTER TO THE EDITOR

Collimated synchrotron threads linking the radio lobes of ESO 137-006

M. Ramatsoku[1,2], M. Murgia[2], V. Vacca[2], P. Serra[2], S. Makhathini[1], F. Govoni[2], O. Smirnov[1,3], L. A. L. Andati[1], E. de Blok[7,5,6], G. I. G. Józsa[3,1,4], P. Kamphuis[9], D. Kleiner[2], F. M. Maccagni[2], D. Cs. Molnár[2], A. J. T. Ramaila[3], K. Thorat[8], and S. V. White[1]

[1] Department of Physics and Electronics, Rhodes University, PO Box 94, Makhanda 6140, South Africa
e-mail: m.ramatsoku@ru.ac.za
[2] INAF – Osservatorio Astronomico di Cagliari, Via della Scienza 5, 09047 Selargius, CA, Italy
[3] South African Radio Astronomy Observatory, 2 Fir Street, Black River Park, 7925 Observatory, South Africa
[4] Argelander-Institut fur Astronomie, Auf dem Hugel 71, 53121 Bonn, Germany
[5] ASTRON, Netherlands Institute for Radio Astronomy, Oude Hoogeveensedijk 4, 7991 PD Dwingeloo, The Netherlands
[6] Department of Astronomy, University of Cape Town, Private Bag X3, 7701 Rondebosch, South Africa
[7] Kapteyn Astronomical Institute, University of Groningen, Postbus 800, 9700 AV Groningen, The Netherlands
[8] Department of Physics, University of Pretoria, Hatfield, Pretoria 0028, South Africa
[9] Ruhr University Bochum, Faculty of Physics and Astronomy, Astronomical Institute, 44780 Bochum, Germany

ABSTRACT

We present MeerKAT 1000 MHz and 1400 MHz observations of a bright radio galaxy in the southern hemisphere, ESO 137-006. The galaxy lies at the centre of the massive and merging Norma galaxy cluster. The MeerKAT continuum images (rms $\sim$0.02 mJy beam^{-1} at $\sim$10$''$ resolution) reveal new features that have never been seen in a radio galaxy before: collimated synchrotron threads of yet unknown origin, which link the extended and bent radio lobes of ESO 137-006. The most prominent of these threads stretches in projection for about 80 kpc and is about 1 kpc in width. The radio spectrum of the threads is steep, with a spectral index of up to $\alpha \simeq 2$ between 1000 and 1400 MHz.

Key words. radio continuum: galaxies

1. Introduction

Radio galaxies residing in galaxy clusters exhibit a wide range of distorted morphologies (see Garon et al. 2019 for an overview). Some of these distortions are seen in the form of head tails, which are elongated radio sources with the galaxy at one end (Ryle & Windram 1968; Sebastian et al. 2017), and wide-angle tails, where the jets form a "C" shape (Owen & Rudnick 1976; Leahy 1993; Missaglia et al. 2019). Such radio morphologies are due to the interaction between the radio lobes and/or jets and the intra-cluster medium (ICM; Pinkney 1995; Sakelliou & Merrifield 2000). This makes radio galaxies important probes of the distribution of pressure, turbulence, and shocks within the magneto-ionic ICM (Owen et al. 2014; Feretti et al. 2012), and also means that their detection is an efficient way to identify high-z clusters independent of dust extinction.

In this Letter we discuss the case of ESO 137-006, a radio galaxy in the Norma galaxy cluster (Abell 3627; Abell et al. 1989). Norma is located at a distance of $\sim$70 Mpc ($z = 0.0162$; Woudt et al. 2008) at the crossing between several filaments in the Great Attractor region (Dressler et al. 1987). With a dynamical mass of $\sim$10^{15} $M_\odot$, Norma is characterised by numerous substructures and exhibits an elongated X-ray morphology, implying that it is not yet in dynamical equilibrium (Boehringer et al. 1996; Woudt et al. 2008).

ESO 137-006 (RA$_{J2000}$ = 16:15:03.8, Dec$_{J2000}$ = –60:54:26) is one of the most luminous galaxies in the Norma cluster and lies near the peak of the X-ray emission. It is one of the brightest radio galaxies in the southern sky ($L_{1.4\,GHz}$ = 2.5 × 10^{25} W Hz^{-1}; Sun 2009). Observations at 408 MHz (Schilizzi & McAdam 1975), 843 MHz (Mauch et al. 2003), and 1400 MHz (Christiansen et al. 1977; Jones & McAdam 1996) show that it has a wide-angle tail morphology. The bending of its radio lobes is thought to be caused by the galaxy infall towards the main cluster (Jones & McAdam 1996; Sakelliou & Merrifield 2000). In this Letter we present new radio continuum images of ESO 137-006 at $\sim$1000 MHz and $\sim$1400 MHz based on MeerKAT observations, which reveal hitherto unseen collimated synchrotron threads (CSTs) between its radio lobes.

Throughout this paper we assume a Λ cold dark matter cosmology with $\Omega_M = 0.3$ and $\Lambda_\Omega = 0.7$, and a Hubble constant of $H_0 = 70$ km s^{-1} Mpc^{-1}. At the distance of ESO 137-006, 1$''$ corresponds to 0.33 kpc.

2. MeerKAT observations and data reduction

We observed the Norma cluster at radio frequencies with MeerKAT (Jonas & MeerKAT Team 2016; Mauch et al. 2020) in May 2019 (project ID SCI-20190418-SM-01). The observations

were conducted with all 64 MeerKAT antennas in *L*-band (856–1712 MHz) using the 4 k mode of the SKARAB correlator, which samples the observed band with 4096 channels, each of 209 kHz in width, in full polarisation. The total integration time is 14 h on target.

We reduced the data in two frequency intervals largely free of radio-frequency interference: 980–1080 MHz and 1356–1440 MHz (hereafter referred to as 1030 MHz and 1398 MHz, respectively). The data reduction was conducted independently in the two intervals using the CARACAL pipeline currently under development[1]. The pipeline is built using STIMELA[2] (Makhathini 2018), a radio interferometry scripting framework based on Python and container technologies. STIMELA allows users to run several open-source radio interferometry software packages in the same script. Using this pipeline, we flagged the calibrator data based on the Stokes *Q* visibilities with AOFLAGGER (Offringa et al. 2010). We determined the complex flux, bandpass, and gains using the CASA (McMullin et al. 2007) tasks *bandpass* and *gaincal*, and applied the calibration to the visibilities of the target with the CASA task *mstransform*. The calibrated target visibilities were flagged with AOFLAGGER, again based on Stokes *Q*. We then iteratively imaged the radio continuum emission with WSCLEAN (Offringa et al. 2014) in Stokes *I* using multi-scale cleaning (Offringa & Smirnov 2017), and self-calibrated the gain phase with CUBICAL (Kenyon et al. 2018) with a solution interval of 128 s. The imaging was done using Briggs *robust* value 0 and cleaning down to 0.5σ within a clean mask made with SOFIA (Serra et al. 2015). Finally, we generated MeerKAT primary beam images at the mean frequency of the two processed bands using EIDOS (Asad et al. 2019), and created primary beam-corrected continuum images of the target.

The resulting 1030 MHz image has a restoring beam of $10.0'' \times 9.1''$ FWHM with PA = 169°, and rms noise level $30.8\,\mu$Jy beam^{-1}. The 1398 MHz image has a restoring beam of $7.5'' \times 6.8''$ FWHM with PA = 167°, and rms noise level $20.8\,\mu$Jy beam^{-1}.

3. ESO 137-006 as seen by MeerKAT

Figure 1 shows the 1030 MHz MeerKAT image of ESO 137-006. Emission shown in red to yellow is known from previous, shallower observations obtained with other telescopes (see Sect. 1). Emission shown in grey scale is revealed here for the first time due to the increased sensitivity and resolution of the MeerKAT data. A number of new features are now apparent.

Similar to earlier observations, we detect a point source corresponding to the galaxy ESO 137-006 (Jones & McAdam 1996). At the resolution of our images this source has a flux density of 140 mJy at 1030 MHz and 167 mJy at 1398 MHz. The source is also seen in X-rays (see Fig. 3) and is thought to be the core of ESO 137-006 (e.g., Jones & McAdam 1996). Narrow jets start from the core along an east–west axis and form two broad, bright spots ~1′ from it. Their peak flux densities are on average ~8 Jy beam^{-1} at 1030 MHz and ~18 Jy beam^{-1} at 1398 MHz. Jones & McAdam (1996) suggested that the brightening and expansion of the jets into these bright spots is due to the decreased ISM pressure. The general structure of these bright spots (see also Fig. 2) is similar to that seen in the hydrodynamical simulations of jets in the FR I radio galaxy 3C 31, where the jets recollimated at ~1.5 kpc from the galaxy core due to the

decreased pressure relative to the ISM after their initial expansion (Perucho & Martí 2007).

Further out, the jets flare into the lobes and then fade into diffuse emission. On both sides, the radio emission bends southwards; in the western lobe the bending occurs right after the bright spot while in the eastern lobe it occurs further out.

Besides the previously known features described immediately above, Fig. 1 shows additional, low-surface-brightness radio emission at the edge of both lobes and, most strikingly, a number of CSTs in the region south of the core. These extend from the lobes southward of the core. Figure 2 shows the gradient image obtained with a Sobel convolution kernel that highlights the presence of three threads: CST1, CST2, and CST3. These threads are reminiscent of twin jets originating from two nuclei associated with radio source 3C 75 (Owen et al. 1985), except for the fact that in the case of ESO 137-006 only one nucleus is seen. Figure 1 also shows a diffuse loop of emission which starts at the base of CST3, extends around the eastern lobe on the south side, and connects back to the lobe on its easternmost side where it fades into diffuse emission. The origin of these features is not known. It is possible that these loops and CSTs are the result of some electromagnetic effect like parallel magnetic field lines within the ICM dragging particles between the lobes as the galaxy moves north, perhaps similar to the description by Heyvaerts & Norman (1989).

The spectral index image ($S_\nu \propto \nu^{-\alpha}$) of ESO 137-006 between 1030 and 1398 MHz is presented in the top panel of Fig. 3. We find a spectral index distribution typical of an active wide-angle tail radio source. The radio core has a flat spectral index $\alpha \simeq 0$ while the inner and brighter parts of the jets have $\alpha \simeq 0.5$–0.6. There is a steepening in the radio spectrum going from the radio lobes down to the tails where we measure a spectral index as high as $\alpha \simeq 4$. The spatial variation of the spectral index in the eastern lobe is more gradual than in the western lobe, where a sharp transition, likely due to projection effects, is observed between the edge of the lobe and the underlying tail emission. The newly discovered CSTs are characterised by a steep radio spectrum with $\alpha \simeq 2$.

In the bottom panel of Fig. 3 we present the MeerKAT image at 1030 MHz superimposed on the X-ray emission map from *XMM-Newton* at 0.5–2 keV. The most relevant feature seen in the X-ray image is a point-like source associated with the radio core and a hint of cavities corresponding to the radio lobes, although no evidence for cavities associated with this source is present in the literature (Shin et al. 2016). At the sensitivity limit of the XMM image, there are no X-ray features that we can associate with these CSTs.

4. Basic properties of CST1

Figure 4 shows the deconvolved full width half maximum ($FWHM_{dec}$) and the peak brightness (I_{peak}) as a function of position along CST1 at 1030 and 1398 MHz, as well as the spectral index ($\alpha^{1398\,MHz}_{1030\,MHz}$). We measure these quantities at the positions shown by the red bars in the inset. The cross in the inset corresponds to the origin of the plot's horizontal axis. Errors were computed using a Monte Carlo simulation with input parameters sampled and noised in the same way as for the real data. The errors represent the scatter of the input versus output best-fit parameters. The mean values of the peak brightness are respectively $I_{peak,1030\,MHz} = (8 \pm 1)$ mJy beam^{-1} and $I_{peak,1398\,MHz} = (4.3 \pm 0.6)$ mJy beam^{-1}, and the average spectral index $\alpha^{1398\,MHz}_{1030\,MHz} = 1.8 \pm 0.3$, consistent with the values shown in Fig. 3.

---

[1] https://caracal.readthedocs.io
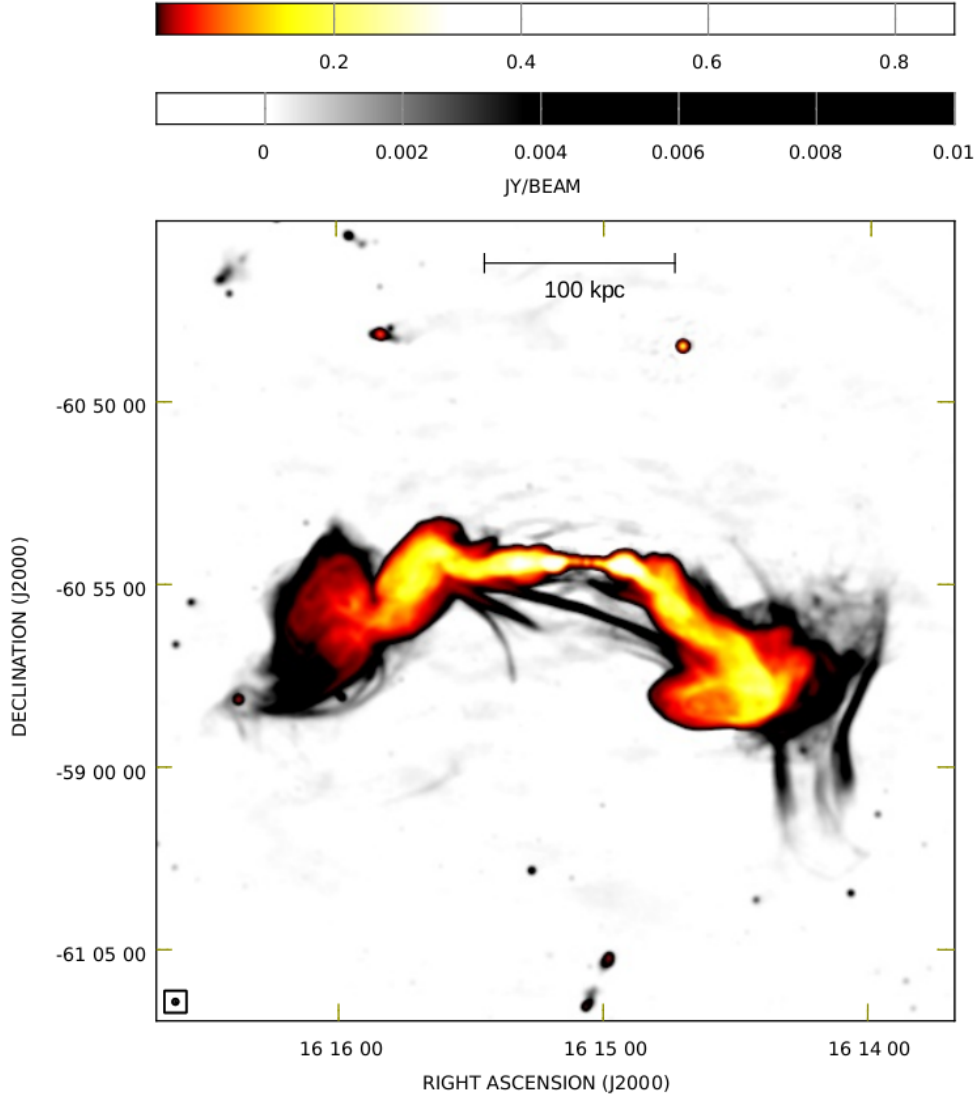[2] https://github.com/SpheMakh/Stimela

Fig. 1. Radio continuum emission from ESO 137-006 detected by MeerKAT at 1030 MHz. The top colour bar (yellow and red tones) represents the brightness of the brighter regions of the radio source in the range from 10 to 860 mJy beam^{-1}. The bottom colour bar (grey tones) represents the brightness of the fainter plumes and filaments in the range from 10 down to −1.6 mJy beam^{-1}. The circular ∼ 10″ synthesised beam of the image is shown in the bottom left corner.
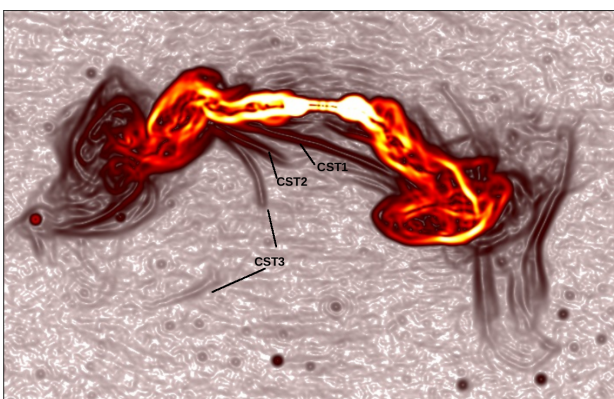

Fig. 2. Gradient image (Sobel convolution kernel) with the three most prominent CSTs labelled.

The peak brightness shows a similar profile at both frequencies, with a valley at ∼60″ at 1030 MHz only, which corresponds to a depression in the spectral index profile. At the same location, a rapid local increase of the deconvolved FWHM can be observed at both frequencies. The mean width of CST1 is $FWHM_{\mathrm{dec,1030\,MHz}} = (3.5 \pm 1.6)''$ and $FWHM_{\mathrm{dec,1398\,MHz}} = (3.5 \pm 1.2)''$. The two profiles do not show any dependence on frequency but are rather characterised by a similar average trend along the full extension of the filament, consistent within the scatter. This projected width translates into 1.2 ± 0.5 kpc, or ∼2% of its 80 kpc length.

5. Discussion and summary

In this Letter we present new MeerKAT images of the radio source ESO 137-006 at 1000 and 1400 MHz. The galaxy lies at the centre of the merging Norma cluster near the Great Attractor. Here we summarise our main findings:

- With these sensitive MeerKAT observations, new features have been revealed in the form of multiple collimated synchrotron threads (CSTs) connecting the lobes of the radio galaxy. It is worth noting that examples of filamentary structures associated with radio galaxies are well known in the literature. However, these filaments are usually observed inside the radio lobes (see e.g. the notable cases of Fornax A and Cygnus A; Maccagni et al. 2020; Perley et al. 1984) and the tails of radio galaxies (e.g., NGC 1265, 3C 129, and NGC 326; Sijbring & de Bruyn 1998; Lane et al. 2002; Hardcastle et al. 2019). The CSTs detected in ESO 137-006 are different in that they are observed outside the main body of the radio galaxy and connecting (at least in projection) the
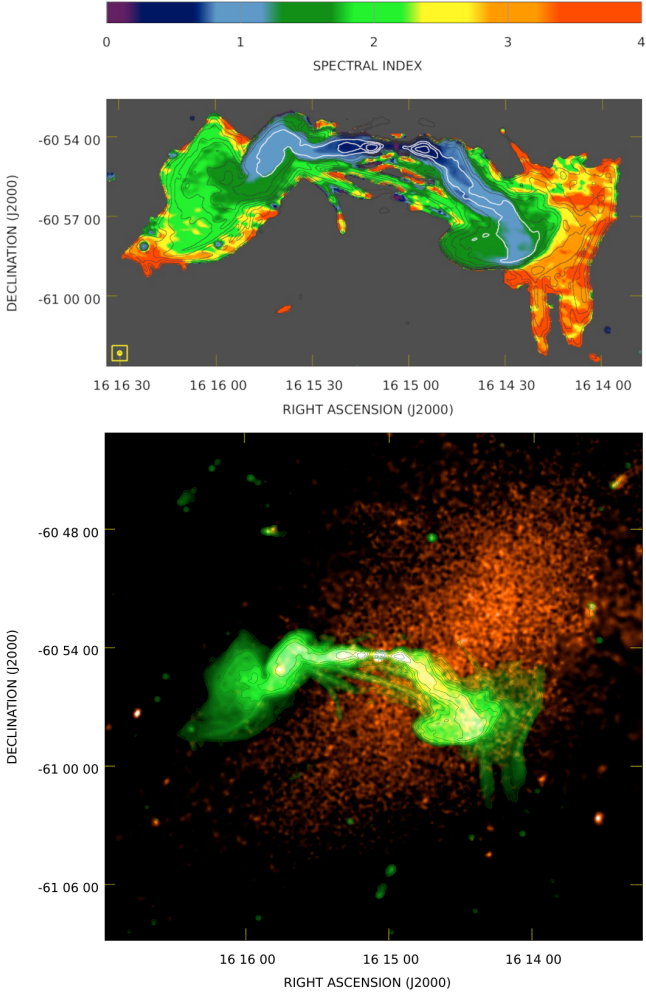
Fig. 3. *Top panel*: spectral index image between 1030 and 1398 MHz. *Bottom panel*: radio continuum emission from ESO 137-006 detected by MeerKAT at 1030 MHz (green tones and contours) superimposed on the X-ray emission map from *XMM-Newton* at 0.5–2 keV. In both panels, radio contours refer to the 1030 MHz image; they start at 0.5 mJy beam^{-1} and scale by a factor of two.

Fig. 4. *Top panel*: spectral index profile between 1030 and 1398 MHz computed along the filament at the locations shown by the slices in the inset (see text for details). *Middle panel*: peak brightness at 1030 MHz (blue triangles) and at 1398 MHz (red triangles) along the filament at the location of the slices. *Bottom panel*: deconvolved FWHM at 1030 MHz (blue dots) and at 1398 MHz (red dots) along the filament at the location of the slices. The plotted error bars are comparable to the size of the dots.

two radio lobes. The radio galaxy 3C 338 (Burns et al. 1983) at the centre of Abell 2199 presents a single filament that is reminiscent of one of the CSTs observed in ESO 137-006. However, while the filament in 3C 338 could be a relic jet from a past epoch of activity, this same interpretation does not hold for ESO 137-006 where we observe multiple close-by threads formed at the same time (as suggested by their similar spectral-index distributions).

– The most prominent and straight of the CST in ESO 137-006 (CST 1) has a characteristic width of ~1 kpc (deconvolved FWHM), roughly 2% of its length, and has a relatively smooth brightness profile with a peak intensity of a few mJy beam^{-1} at the 10″ resolution of our images. The other two CSTs originate from the same point in the eastern lobe. CST 2 starts straight and then fades rapidly after ~25 kpc from the lobe. CST 3 seems to follow a faint, closed loop with a radius of ~64 kpc, which reconnects with the lobe at its far end. The nature of these unusual features is unclear. We speculate that they could be due to the interaction of the magnetic fields of the radio lobes with the magneto-ionic ICM, or caused by some sort of re-connection of filaments
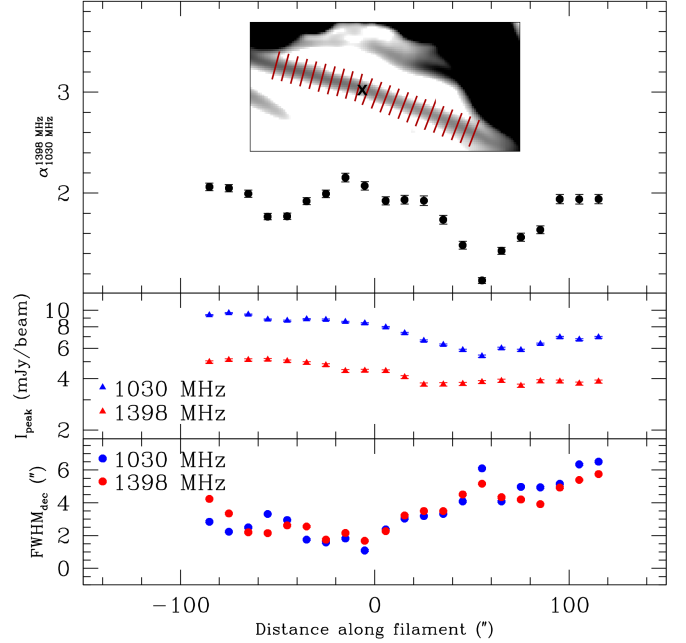
associated with the tails back into the radio lobes. Further observations and theoretical efforts are required to clarify the nature of these newly discovered features.

– The spectral index distribution observed across the jets, lobes, and tails is typical of an active radio source. The radio spectrum of the CST is steep with $\alpha \simeq 2$. Due to this steep spectrum, deep low-frequency observations at high resolution with instruments such as the LOw Frequency ARray could play a role in the study of CSTs.

– Whatever their origin, our findings pose the following questions: How common are these features? Are CSTs specific to the case of ESO 137-006 and its environment, perhaps due to the kinematics and pressure gradient of this ICM and relative motion of the galaxy in the cluster? Or, on the contrary, are CSTs common in radio galaxies but have so far not been detected due to sensitivity and resolution limits? If future observations confirm the latter hypothesis, understanding the nature and the physics of these features could open a new science case for the next generation of sensitive radio interferometers like the Square Kilometre Array.

References

Abell, G. O., Corwin, H. G., Jr, & Olowin, R. P. 1989, ApJS, 70, 1
Asad, K. M. B., Girard, J. N., de Villers, M., et al. 2019, MNRAS, submitted [arXiv:1904.07155]
Boehringer, H., Neumann, D. M., Schindler, S., & Kraan-Korteweg, R. C. 1996, ApJ, 467, 168
Burns, J. O., Schwendeman, E., & White, R. A. 1983, ApJ, 271, 575
Christiansen, W. N., Frater, R. H., Watkinson, A., et al. 1977, MNRAS, 181, 183
Dressler, A., Faber, S. M., Burstein, D., et al. 1987, ApJ, 313, L37
Feretti, L., Giovannini, G., Govoni, F., & Murgia, M. 2012, A&ARv, 20, 54
Garon, A. F., Rudnick, L., Wong, O. I., et al. 2019, AJ, 157, 126
Hardcastle, M. J., Croston, J. H., Shimwell, T. W., et al. 2019, MNRAS, 488, 3416
Heyvaerts, J., & Norman, C. 1989, ApJ, 347, 1055
Jones, P. A., & McAdam, W. B. 1996, MNRAS, 282, 137
Jonas, J., & MeerKAT Team. 2016, in MeerKAT Science: On the Pathway to the SKA, 1
Kenyon, J. S., Smirnov, O. M., Grobler, T. L., & Perkins, S. J. 2018, MNRAS, 478, 2399
Lane, W. M., Kassim, N. E., Ensslin, T. A., Harris, D. E., & Perley, R. A. 2002, AJ, 123, 2985
Leahy, J. P. 1993, in DRAGNs, eds. H. J. Röser, & K. Meisenheimer, 421, 1
Maccagni, F. M., Murgia, M., Serra, P., et al. 2020, A&A, 634, A9
Makhathini, S. 2018, Ph.D. Thesis, Rhodes University, Drosty Rd, Grahamstown, 6139, Eastern Cape, South Africa
Mauch, T., Murphy, T., Buttery, H. J., et al. 2003, MNRAS, 342, 1117
Mauch, T., Cotton, W. D., Condon, J. J., et al. 2020, ApJ, 888, 61
McMullin, J. P., Waters, B., Schiebel, D., Young, W., & Golap, K. 2007, in Astronomical Data Analysis Software and Systems XVI, eds. R. A. Shaw, F. Hill, & D. J. Bell, ASP Conf. Ser., 376, 127
Missaglia, V., Massaro, F., Capetti, A., et al. 2019, A&A, 626, A8
Offringa, A. R., & Smirnov, O. 2017, MNRAS, 471, 301
Offringa, A. R., de Bruyn, A. G., Biehl, M., et al. 2010, MNRAS, 405, 155
Offringa, A. R., McKinley, B., Hurley-Walker, N., et al. 2014, MNRAS, 444, 606
Owen, F. N., & Rudnick, L. 1976, ApJ, 205, L1
Owen, F. N., O'Dea, C. P., Inoue, M., & Eilek, J. A. 1985, ApJ, 294, L85
Owen, F. N., Rudnick, L., Eilek, J., et al. 2014, ApJ, 794, 24
Perley, R. A., Dreher, J. W., & Cowan, J. J. 1984, ApJ, 285, L35
Perucho, M., & Martí, J. M. 2007, MNRAS, 382, 526
Pinkney, J. 1995, Ph.D. Thesis, New Mexico State University, USA
Ryle, M., & Windram, M. D. 1968, MNRAS, 138, 1
Sakelliou, I., & Merrifield, M. R. 2000, MNRAS, 311, 649
Schilizzi, R. T., & McAdam, W. B. 1975, MmRAS, 79, 1
Sebastian, B., Lal, D. V., & Pramesh Rao, A. 2017, AJ, 154, 169
Serra, P., Westmeier, T., Giese, N., et al. 2015, MNRAS, 448, 1922
Shin, J., Woo, J.-H., & Mulchaey, J. S. 2016, ApJS, 227, 31
Sijbring, D., & de Bruyn, A. G. 1998, A&A, 331, 901
Sun, M. 2009, ApJ, 704, 1586
Woudt, P. A., Kraan-Korteweg, R. C., Lucey, J., Fairall, A. P., & Moore, S. A. W. 2008, MNRAS, 383, 445